2025 IEEE/SICE International Symposium on System Integration (SII)
January 21-24, 2025, Munich, Germany

Real-Time Calculation of Strain Energy Density in a Fingertip for Haptic Distribution Rendering

Kazuya Sase[1], Haruki Kato[2], Hikaru Nagano[3], and Masashi Konyo[4]

Abstract— **Considering the neural signals generated by mechanoreceptors in response to haptic stimuli when contacting virtual objects is essential to display spatial haptic distributions on the skin in virtual reality applications. This study focuses on reproducing the neural activities of Merkel cells, which are known as slowly adapting type-1 mechanoreceptors. The firing activity of these receptors is known to respond to strain energy density (SED). We developed a real-time SED calculation method using a specially designed finite element (FE) model of a fingertip, which features a simplified layer structure of skin and nail. We validated the model by comparing its calculation results with those of a detailed model and a homogeneous model, using reliable FE analysis software. We demonstrated that modeling the layered structure of the skin is effective in improving the reproducibility of the SED distribution at the locations of Merkel cells.**

I. INTRODUCTION

Humans have mechanoreceptors beneath the skin surface that are believed to encode various types of contact information generated by touching objects. These receptors are activated when the surrounding local structures are mechanically deformed or stressed. Analyzing the neural activity of these receptors is crucial not only for understanding how humans perceive the sense of touch but also for reproducing convincing haptic stimuli in virtual reality (VR) environments.

Merkel cells are a type of mechanoreceptor known as slowly adapting type-1 (SA1) receptors. They respond to slow mechanical stimuli, such as static pressure and low-frequency vibrations, and have small receptive fields that enable the detection of fine contact information. These cells are densely distributed across the human skin, particularly at the fingertips. They are believed to be essential in shape recognition and material identification. The firing rate of Merkel cells appears to be related to the strain energy density (SED) at their locations [1]. Therefore, understanding the SED distribution in a fingertip is valuable.

Researchers in the haptics community have studied haptic distribution displays. To utilize these displays, a software is needed to compute the control signals required for displaying appropriate haptic stimuli, a process commonly referred to as haptic rendering. To accurately reproduce the sense of touch in a specific situation, haptic stimuli that generate neural activities closely matching those that occur in the real-world scenario should be displayed.

This study proposes a method for calculating the SED distribution in a finger, with the future goal of reproducing the neural activities of SA1 receptors. To realize this method in VR applications, the calculation must be performed in real time. To this end, we developed a finite element (FE) model of a finger that can be calculated in real time. A fast implementation of the finite element method (FEM) is adopted. We evaluated the results of our implementation by comparing them with accurate simulation results obtained using reliable finite element analysis (FEA) software.

II. RELATED WORKS

Haptic distribution displays for a finger pad have been extensively developed. Pin-array displays are the most classic tactile displays, and the earliest ones were developed to assist the visually impaired [2]. In recent years, wearable pin-array displays have been developed and their density and coverage area have been improving [3]. Suction pressure can be used for tactile distribution display. The authors developed a high-resolution haptic display that applies suction pressure to a finger pad from suction holes aligned densely [4]. Electrotactile stimulation is also adopted for haptic distribution display by generating electrical stimuli from aligned electrodes [5]. Airborne ultrasound haptic displays have made significant progress, and pressure distribution presentation has recently been addressed [6].

Haptic display requires not only the device but also the computation of haptic information. Such a computational process is known as haptic rendering. In most device studies, haptic rendering is limited to the drawing of primitive shapes such as simple lines for device evaluation [7]. In pin-array type devices, an approach exists that mimics the shape of the target object as it is [8]. However, physical interactions involving motion or deformation of the target object are difficult to achieve by simply simulating its shape. To achieve more diverse interactions, physical simulation is used. The authors proposed a calculation method of pressure distribution on a finger pad [9]. In the study, the suction pressure distribution was presented by applying a gain to the calculated contact pressure. A method exists to calculate the interaction between the fluid and hand in real time and seek a focal point that approaches that pressure distribution to the maximum extent on the ultrasonic display [10]. For a wearable pin-array display, a method has been developed to determine the pin force to achieve the target skin deformation

*This work was supported by JSPS KAKENHI Grant Numbers JP21H04542, JP22K17936 and JP23H00480.

[1]Kazuya Sase is with Faculty of Engineering, Tohoku Gakuin University, Sendai, Japan sase@mail.tohoku-gakuin.ac.jp

[2]Haruki Kato is with Graduate School of Engineering, Tohoku Gakuin University, Sendai, Japan

[3]Hikaru Nagano is with Graduate School of Science and Technology, Kyoto Institute of Technology, Kyoto, Japan

[4]Masashi Konyo is with Graduate School of Information Sciences, Tohoku University, Sendai, Japan

through optimization calculations [11]. Some researchers have focused on SED at mechanoreceptor locations and generated SED-based control signals [12]. This is an important concept in reproducing the mechanism through which people feel tactile sensations.

Some human mechanoreceptors are known to respond to SED [1]. Knowing the firing activity of receptors when a person touches an object is important for a better understanding of human perception. Therefore, attempts have been made to construct a biomechanical model of the human finger and to calculate subcutaneous SED distribution by simulating deformation [13]. However, to the best of our knowledge, no study has been realized to compute SED by real-time computation of finger deformations.

In contrast, several studies have been conducted to calculate hand skin deformations in real time [14], [15]. However, they focused on the visual quality of skin deformation and interaction with objects in VR. Therefore, the heterogeneous subcutaneous anatomy has not garnered significant attention. This study is the first attempt to compute the deformation of an FE model that reproduces the layered structure of the skin and obtain the SED at the receptor location in real time.

III. CALCULATION METHOD

A. Finite Element Model

The FE model of a fingertip was constructed based on a three-dimensional model of an index fingertip, extracted from a computed tomography image of the right hand of an adult male [16]. We initially attempted to model the fingertip with maximum details, including the stratum corneum, epidermis, dermis, subcutaneous tissue, bone, and nail. The model is shown in Fig. 1(a), hereinafter referred to as Model A. The stratum corneum is modeled using triangular shell elements, whereas the other parts are modeled using tetrahedral elements. The thicknesses values of the skin layers are listed in Table I. Although this model accurately reflects the structure of a human finger, simulating the mechanical behavior of such a detailed model in real time is challenging. Therefore, this detailed model is utilized for evaluation purposes and not for real-time simulation.

To enable real-time calculation of finger deformation, the model was simplified. The simplified model is shown in Fig. 1(b), hereinafter referred to as Model B. It comprises the epidermis, dermis, subcutaneous tissue, bone, and nail. The layer thickness was slightly increased as summarized in Table I, and the stratum corneum layer was omitted, as modeling such a thin structure would require extremely large number of tetrahedral elements. The bone and nail are combined and treated as a rigid body. The model contains 1554 nodes and 7244 tetrahedral elements, excluding bone and nail parts. For comparison, a homogeneous model was also constructed (Fig. 1(c), hereinafter referred to as Model C). In this model, all tissues except those for the bone are modeled as homogeneous soft tissues. This assumption is commonly used in real-time applications such as in [14], that is, it is a conventional approach.

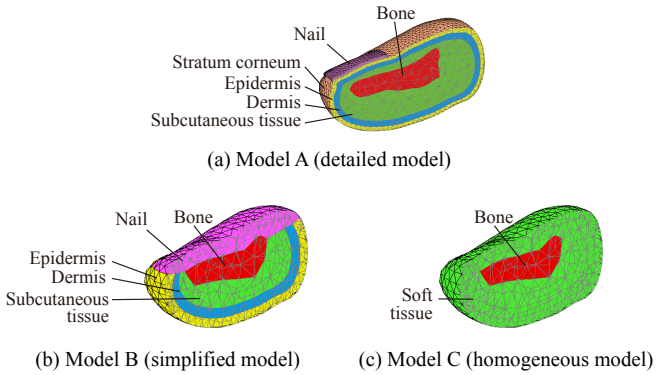

(a) Model A (detailed model)

(b) Model B (simplified model)

(c) Model C (homogeneous model)

Fig. 1. Cross-sectional views of the FE models: (a) Model A (detailed model), (b) Model B (simplified model), (c) Model C (homogeneous (oversimplified) model commonly used in real-time applications). See Fig. 3 for an overall view of Model A.

TABLE I

THICKNESS OF SKIN LAYERS (UNIT: MM) [17]

	Mode A	Model B
Stratum corneum	0.02	-
Epidermis	1.0	1.5
Dermis	0.75	3.0

The material properties used in this model are listed in Table II. The soft tissues (epidermis, dermis, and subcutaneous tissue) are modeled as linear elastic materials [17]. In the homogeneous model, the material properties of the subcutaneous tissue are used for the entire soft tissue.

B. Real-time Simulation Method

In the proposed method, deformation is calculated using corotational linear FEM, which is fundamentally similar to the linear FEM framework but considers element rotation to account for geometric nonlinearity. Time evolution is calculated using the backward Euler method to ensure high stability. The attachment between the rigid body (bone and nail) and soft tissue is implemented using the penalty method, where spring-damper elements connect them (Fig. 2(a)). This allows for the movement of the entire finger, including the skin, to be represented by synchronizing the bone positions with the data obtained from sensors. We also represent the contact between objects using the penalty method (Fig. 2(b)). The effects of these penalty methods are also reflected in the stiffness matrix to improve stability. Pseudo friction is represented by anisotropic springs. Collision detection is implemented using a signed distance field. When the vertices of the mesh intersect with a rigid object, they are repelled to the surface of the collided object. The computation is partially parallelized for multi-core CPUs to accelerate processing. Because a considerable portion this calculation method is based on the author's previous study, please refer to [18] for details.

The SED distribution at the receptors is calculated at the interface between the dermis and epidermis because Merkel cells are located in the basal epidermal layer. In the current FEM framework, we use only isotropic elastic elements.

TABLE II

MATERIAL PROPERTIES OF A FINGER MODEL [17].

Components	E [MPa]	ν [-]	ρ [g/cm^3]
Bone	1.700×10^{4}	0.30	1.8
Subcutaneous tissue	3.400×10^{-2}	0.48	1.0
Dermis	8.000×10^{-2}	0.48	1.0
Epidermis	1.360×10^{-1}	0.48	1.0
Stratum corneum	1.993	0.48	1.1
Nail	1.700×10^{2}	0.30	1.8

E, ν, and ρ are Young's modulus, Poisson's ratio, and density, respectively.

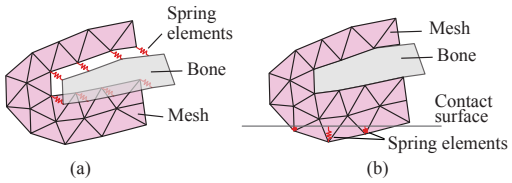

Fig. 2. Overview of the penalty method. (a) connection between bone and soft tissue. (b) contact with object surface.

Thus, the SED of an element can be calculated as follows:

$$SED = \frac{1}{2}\sum_{i,j}\sigma_{ij}\epsilon_{ij}, \tag{1}$$

where σ_{ij} and ϵ_{ij} denote the components of the stress and strain tensors of the element, respectively. After the SED values on the elements are obtained, the SED at a vertex is calculated by averaging the values of the elements connected to the vertex.

In a real-time application, the fingertip model can be moved by tracking the user's finger and applying the motion to the bone position and orientation. The calculated SED can be converted into control signals for the haptic display, for instance, suction pressure in [4] or intensity of electrical stimulation in [12].

IV. EVALUATION

A. Conditions

We evaluated the models described in Sec. III-A by performing simulations and comparing the results. To validate the models, we used the FEA software MSC Marc Mentat 2022.3 and analyzed mechanical behavior while a model is pressed against a rigid plane. The simulation conditions are described in Fig. 3. The finger model is tilted 15° relative to the plane, and eight nodes of the bone part are fixed. The plane is pressed vertically into the finger pad by 2.0 mm over 50 steps. A four-node tetrahedron with strain smoothing (Element 242 in the Marc Element Library) was used for the elements of the FE mesh of the finger. This element uses piecewise trilinear interpolation functions and an enhanced integration scheme that enforces strain smoothing over neighboring elements. FEA was performed using a large strain static analysis scheme without friction. The analysis calculates the reaction force between the plane and the finger pad, contact area, and SED distribution on the

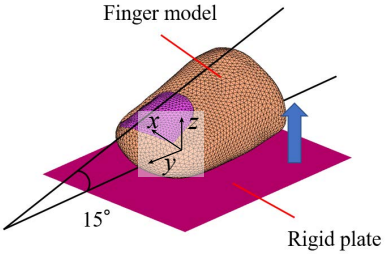

Fig. 3. Simulation condition.

surface of the dermis, which is considered the location of Merkel cells.

Real-time simulation was also performed to evaluate the proposed method described in Sec. III-B. Only Model B in Fig. 1 was used for real-time simulation. The simulation conditions are the same as those used in Marc. The parameters of the penalty method were set as follows: spring coefficient $k_{bone} = 200$ [N/m], damper coefficient $b = 0.1$ [N·s/m], anisotropy factor $a_{bone} = 1.0$ (no anisotropy) for bone connection, and spring coefficient $k_{contact} = 10000$ [N/m], damper coefficient $b = 0.5$ [N·s/m], and anisotropy factor $a_{bone} = 0.0$ (no shear stiffness, that is, no friction) for contact response. The total contact force is calculated by summing the spring forces. A tetrahedral linear element was used for the FE mesh. The computer used for the real-time simulation is equipped with an Intel Core i9-11900KF CPU (8 cores, 3.5–5.3 GHz), 32 GB RAM, an NVIDIA RTX 3090 GPU (used only for graphics rendering), and Ubuntu 22.04 OS. The calculation software was implemented in C++ with OpenMP for CPU parallelization.

B. Visual Appearance, Stability, and Performance

All simulations were performed stably, without vibration or divergence. The deformations obtained from the simulation using Model A (Marc) and Model B (real-time simulation) are shown in Figs. 4 and 5, respectively. The real-time simulations accurately handled contact with the rigid plane and generated plausible deformations based on the stiffness distributions of the inner layered material structures. The real-time simulation was performed at approximately 50 fps, which is visually smooth and should cover a wide range of frequencies for slow haptic phenomena such as pushing and stroking.

C. Validation

Here, we assume that the results of the simulation using the detailed model (Model A) are the ground truth. Therefore, the validity of the results from the other models is evaluated by measuring the error relative to those of the detailed model.

1) Force and contact area: Fig. 6 shows the relationship between pushing displacement and reaction force. The force measured in Model B (Marc) is always higher than that in Model A. This indicates that the overall stiffness of Model B is higher than that of Model A. The higher stiffness is considered to result from the simplified structure, which

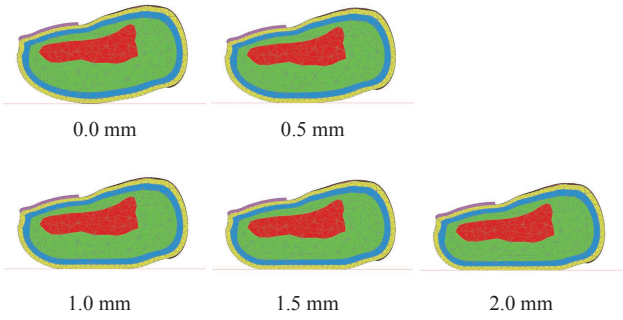

Fig. 4. Deformation results of the simulation with Marc.

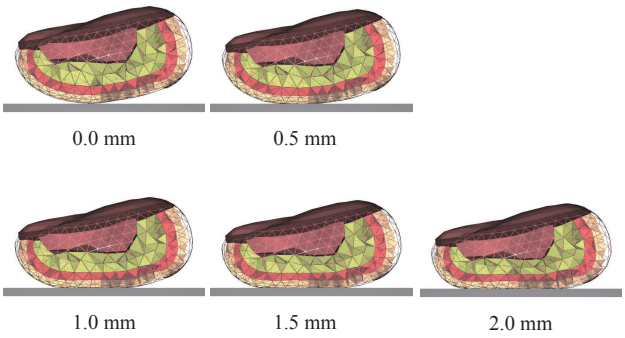

Fig. 5. Deformation results of the real-time simulation.

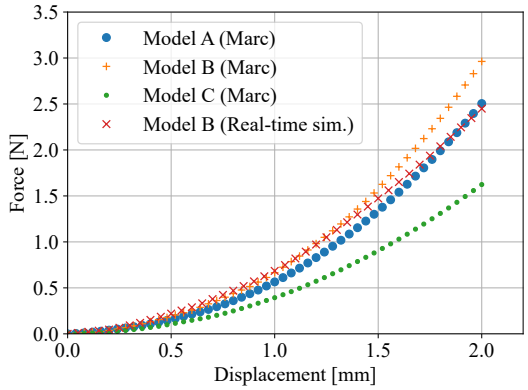

Fig. 6. Force vs. displacement.

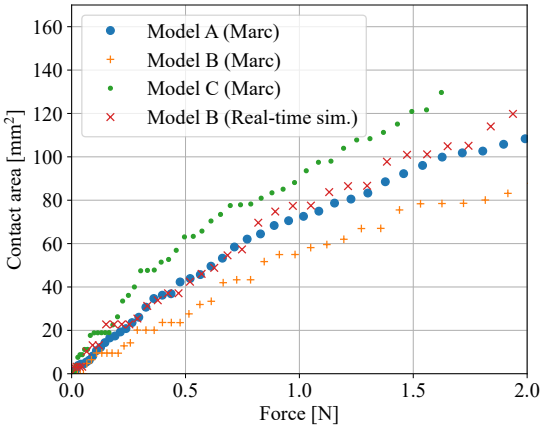

Fig. 7. Contact area vs. force.

includes a large volume of rigid parts (nail and bone) and thick, stiff skin layers (epidermis and dermis). In contrast, Model C is softer than the others owing to its simple, homogeneous soft structure. Fig. 7 shows the relationship between force and contact area. The contact area became larger as the model became softer, as expected.

The real-time simulation of Model B exhibited softer behavior, particularly when the displacement exceeded 1.5 mm, compared to the results from Model B (Marc). This could be because of the soft constraints introduced by the penalty method. The contact area appeared to be affected by the soft constraints, as it is larger than that in the results from Marc. When comparing Model B (real-time simulation) with Model A (Marc), the force and contact area are similar. However, this is considered to be the result of the soft behavior in the real-time simulation and is not a desirable property.

2) SED distribution: Figs. 8 and 9 show the SED distributions across the sagittal and coronal sections, respectively. The distributions are overlaid on the material structures. The SED distributions shown are the results of displacements that bring the force closest to 1.0 N. The SED distribution of Model C had the highest value among the models because it is the softest and most extensively deformed. In Models A and B, SED tends to accumulate in the softest parts, such as the soft tissues. In contrast, SED is generally smaller in the stiffer parts, such as the dermis and epidermis.

The SED distributions at the location of Merkel cells under a force of 1.0 N are shown in Fig. 10. These contour plots are developed using the SED values of vertices on the interface surface between the epidermis and dermis. In each contour plot, the maximum SED value is annotated. The maximum SED values differ significantly from each other. In particular, Model C exhibited the highest SED value, followed by Model B.

For a more quantitative comparison, the path plots of the SED distributions are shown in Fig. 11. These plots were developed along the x-axis at $y = 2$, around the periphery of the SED peak. Fig. 12 shows the normalized SED distribution, developed by dividing the SED values by the maximum SED values obtained from Fig. 10. We measured the errors of each model relative to Model A (Table III). The error measurements revealed that Model B had the smallest mean absolute error. Consequently, its distribution shape was relatively close to that of Model A and provided a better approximation than Model C. This finding supports that incorporating skin layers positively impacts the accuracy of SED calculations for Merkel cells.

Finally, when comparing the SED distribution of Model B

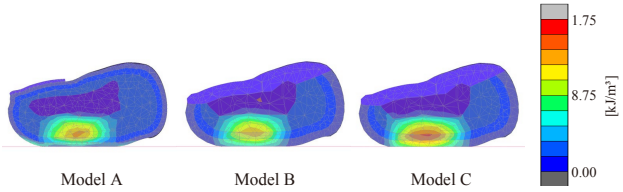

Fig. 8. SED distributions across sagittal sections ($x = 0$) at a force of 1.0 N calculated by Marc.

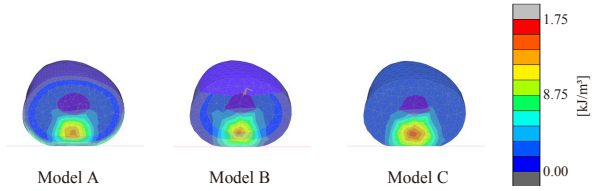

Fig. 9. SED distributions across coronal sections ($y = 2$) at a force of 1.0 N calculated by Marc.

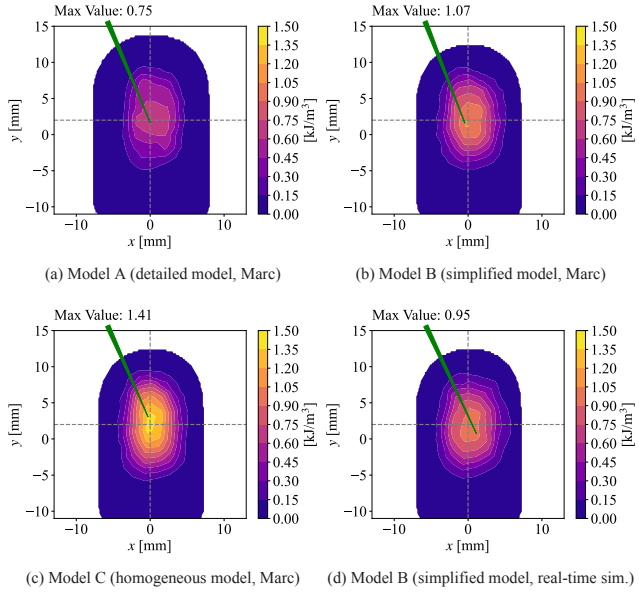

(a) Model A (detailed model, Marc)

(b) Model B (simplified model, Marc)

(c) Model C (homogeneous model, Marc)

(d) Model B (simplified model, real-time sim.)

Fig. 10. SED distributions at the location of Merkel cells under a force of 1.0 N.

(real-time simulation) with that of Model B (Marc), the real-time simulation exhibits a smoother distribution. This may be owing to the soft constraints and use of lower-precision FEs in the calculation method. However, this effect was minor, and as summarized in Table III, the real-time simulation exhibited smaller errors compared to the homogeneous model (Model C). Therefore, this method is more accurate than the commonly used homogeneous model and is effective for real-time SED calculation.

V. CONCLUSIONS

This study proposed a real-time method for calculating SED distributions to render haptic feedback for SA1 receptors. We developed a simplified FE model of skin

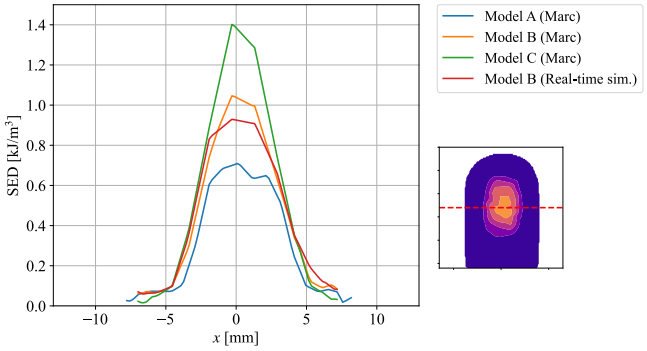

Fig. 11. Path plot of SED along x axis ($y = 2$).

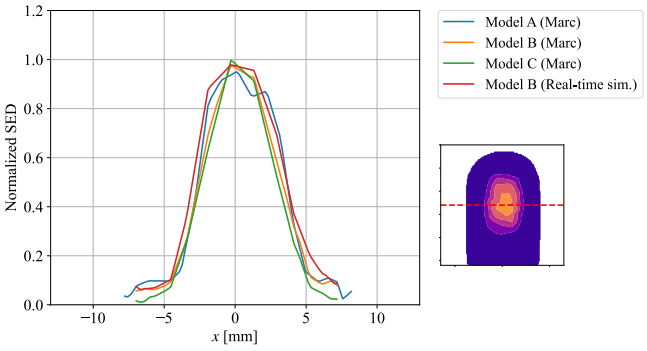

Fig. 12. Path plot of normalized SED along x axis ($y = 2$). The SED values in Fig. 11 are normalized by the maximum value of each SED distribution shown in Fig. 10.

TABLE III
ERRORS IN THE NORMALIZED PATH PLOTS FOR MODEL A.

	Mean abs. err.	Max. abs. err.
Model B (Marc)	**0.044**	0.152
Model C (Marc)	0.073	0.215
Model B (Real-time Sim.)	0.050	**0.132**

anatomy for finger deformation calculations, and SED values at Merkel cell locations were obtained using an accelerated FE method. The real-time simulations were stable and performed at 50 fps. Furthermore, to validate the calculation results for flat finger pressing, we compared them with FEA results from a detailed finger model and confirmed that the proposed model calculates the SED distribution with higher accuracy than the commonly used homogeneous model. We believe that this method allows us to generate appropriate control signals for haptic distribution displays, effectively reproducing the neural activities of Merkel cells.

In the future, we intend to evaluate the accuracy of finger deformation and SED distribution when interacting with objects of different shapes and material properties, as well as under various touching styles, to improve the model. Additionally, we are considering applying the model to VR applications and to robotic teleoperation, where tactile sensor measurements from a follower robotic finger could be used to generate an equivalent SED for a human leader finger.

ACKNOWLEDGMENT

The authors would like to thank Dr. Mitsunori Tada, National Institute of Advanced Industrial Science and Technology, for providing a fingertip model.

REFERENCES

[1] M. A. Srinivasan and K. Dandekar, "An Investigation of the Mechanics of Tactile Sense Using Two-Dimensional Models of the Primate Fingertip," *Journal of Biomechanical Engineering*, vol. 118, no. 1, pp. 48–55, 02 1996. [Online]. Available: https://doi.org/10.1115/1.2795945

[2] J. C. Bliss, "A relatively high-resolution reading aid for the blind," *IEEE Transactions on Man-Machine Systems*, vol. 10, no. 1, pp. 1–9, 1969.

[3] Y. Ujitoko, T. Taniguchi, S. Sakurai, and K. Hirota, "Development of finger-mounted high-density pin-array haptic display," *IEEE Access*, vol. 8, pp. 145 107–145 114, 2020.

[4] N. Morita, A. Ichijo, M. Konyo, H. Kato, K. Sase, H. Nagano, and S. Tadokoro, "Wearable high-resolution haptic display using suction stimuli to represent cutaneous contact information on finger pad," *IEEE Transactions on Haptics*, vol. 16, no. 4, pp. 687–694, 2023.

[5] K. Sato and S. Tachi, "Design of electrotactile stimulation to represent distribution of force vectors," in *2010 IEEE Haptics Symposium*, 2010, pp. 121–128.

[6] A. Matsubayashi, Y. Makino, and H. Shinoda, "Rendering ultrasound pressure distribution on hand surface innbsp;real-time," in *Haptics: Science, Technology, Applications: 12th International Conference, EuroHaptics 2020, Leiden, The Netherlands, September 6–9, 2020, Proceedings*. Berlin, Heidelberg: Springer-Verlag, 2020, p. 407–415.

[7] S.-C. Kim, C.-H. Kim, G.-H. Yang, T.-H. Yang, B.-K. Han, S.-C. Kang, and D.-S. Kwon, "Small and lightweight tactile display(salt) and its application," in *World Haptics 2009 - Third Joint EuroHaptics conference and Symposium on Haptic Interfaces for Virtual Environment and Teleoperator Systems*, 2009, pp. 69–74.

[8] D. Leithinger, D. Lakatos, A. DeVincenzi, M. Blackshaw, and H. Ishii, "Direct and gestural interaction with relief: a 2.5d shape display," in *Proceedings of the 24th Annual ACM Symposium on User Interface Software and Technology*, ser. UIST '11. New York, NY, USA: Association for Computing Machinery, 2011, p. 541–548.

[9] H. Nagano, K. Sase, M. Konyo, and S. Tadokoro, "Wearable suction haptic display with spatiotemporal stimulus distribution on a finger pad," in *2019 IEEE World Haptics Conference (WHC)*, 2019, pp. 389–394.

[10] H. Barreiro, S. Sinclair, and M. A. Otaduy, "Ultrasound rendering of tactile interaction with fluids," in *2019 IEEE World Haptics Conference (WHC)*, 2019, pp. 521–526.

[11] K. Hirota, Y. Ujitoko, S. Sakurai, and T. Nojima, "Deformation matching: Force computation based on deformation optimization," *IEEE Transactions on Haptics*, vol. 15, no. 2, pp. 267–279, 2022.

[12] K. Sato, H. Nii, N. Kawakami, and S. Tachi, "Electrotactile stimulation based on strain energy density of the fingertip," in *Haptics: Perception, Devices and Scenarios*, M. Ferre, Ed. Berlin, Heidelberg: Springer Berlin Heidelberg, 2008, pp. 724–729.

[13] T. Hamasaki and D. Yamada, "Mechano-neurophysiological model of the fingertip for spatiotemporal firing pattern prediction of sa1 mechanoreceptors during embossed letter scanning," *Advances in Mechanical Engineering*, vol. 13, no. 2, p. 1687814020984651, 2021. [Online]. Available: https://doi.org/10.1177/1687814020984651

[14] K. Hirota and K. Tagawa, "Interaction with virtual object using deformable hand," in *2016 IEEE Virtual Reality (VR)*, 2016, pp. 49–56.

[15] M. Verschoor, D. Lobo, and M. A. Otaduy, "Soft hand simulation for smooth and robust natural interaction," in *2018 IEEE Conference on Virtual Reality and 3D User Interfaces (VR)*, 2018, pp. 183–190.

[16] T. Nakajima, Y. Asami, Y. Endo, M. Tada, and N. Ogihara, "Prediction of anatomically and biomechanically feasible precision grip posture of the human hand based on minimization of muscle effort," *Scientific Reports*, vol. 12, no. 1, p. 13247, Aug 2022. [Online]. Available: https://doi.org/10.1038/s41598-022-16962-1

[17] T. Maeno, K. Kobayashi, and N. Yamazaki, "Relationship between the structure of human finger tissue and the location of tactile receptors," *JSME International Journal Series C*, vol. 41, no. 1, pp. 94–100, 1998.

[18] K. Sase, T. Tsujita, and A. Konno, "Haptic rendering of contact between rigid and deformable objects based on penalty method with implicit time integration," in *2016 IEEE International Conference on Robotics and Biomimetics (ROBIO)*, 2016, pp. 1594–1600.